

Combining SELEX Screening and Rational Design to Develop Light-Up Fluorophore–RNA Aptamer Pairs for RNA Tagging

Jungjoon Lee^{†,§}, Kyung Hyun Lee^{‡,§}, Jongho Jeon^{‡,§}, Anca Dragulescu-Andrasi[‡], Fei Xiao[‡], and Jianghong Rao^{†,*,*}

[†]Department of Chemistry and [‡]Molecular Imaging Program at Stanford (MIPS), Department of Radiology, Stanford University School of Medicine, 1210 Welch Road, Stanford, California 94305-5484. [§]These authors contributed equally to this work.

Site-specific labeling of proteins with molecular tags has been widely used to study structure and function of proteins and for the direct visualization of protein dynamics, localization, and interactions in single living cells (1–5). The proteins of interest can be labeled by genetic fusions to fluorescent proteins or chemical reactions with fluorescent dyes. With the important role of RNA molecules in biology, there is strong interest in applying the specific labeling strategy to RNA molecules (6–8). This extension is however challenging because there is no RNA counterpart of green fluorescent proteins (GFPs) and there are limited chemical functional groups in RNA molecules available for specific chemical labeling.

The straightforward RNA tagging approach is to attach fluorophores to oligonucleotides complementary to the target RNA molecules. This technique is commonly used in fluorescent *in situ* hybridization (FISH) for imaging target mRNA in fixed cells and tissues (9–13). To improve the sensitivity in detecting a low abundant RNA target, oligonucleotides may be labeled with an additional quencher or dye molecule to form “molecular beacons” so that the probe is quenched in an “off” state and turns on after forming a complex with the target RNA (6, 8, 14–17). Another strategy similar to molecular beacons uses the target RNA as the template to direct the ligation of two complementary oligonucleotides, resulting in the activation of the probe from fluorescently quenched to emitting states (18, 19). Because of the negatively charged backbone of the nucleotides, this type of fluorescent probes is generally not cell-permeable and demonstrates poor delivery for

ABSTRACT We report here a new small molecule fluorogen and RNA aptamer pair for RNA labeling. The small-molecule fluorogen is designed on the basis of fluorescently quenched sulforhodamine dye. The SELEX (Systematic Evolution of Ligands by EXponential enrichment) procedure and fluorescence screening in *E. coli* have been applied to discover the aptamer that can specifically activate the fluorogen with micromolar binding affinity. The systematic mutation and truncation study on the aptamer structure determined the minimum binding domain of the aptamer. A series of rationally modified fluorogen analogues have been made to probe the interacting groups of fluorogen with the aptamer. These results led to the design of a much improved fluorogen ASR 7 that displayed a 33-fold increase in the binding affinity for the selected aptamer in comparison to the original ASR 1 and an 88-fold increase in the fluorescence emission after the aptamer binding. This study demonstrates the value of combining *in vitro* SELEX and *E. coli* fluorescence screening with rational modifications in discovering and optimizing new fluorogen–RNA aptamer labeling pairs.

*Corresponding author,
jrao@stanford.edu.

Received for review June 27, 2010
and accepted August 31, 2010.

Published online September 1, 2010

10.1021/cb1001894

© 2010 American Chemical Society

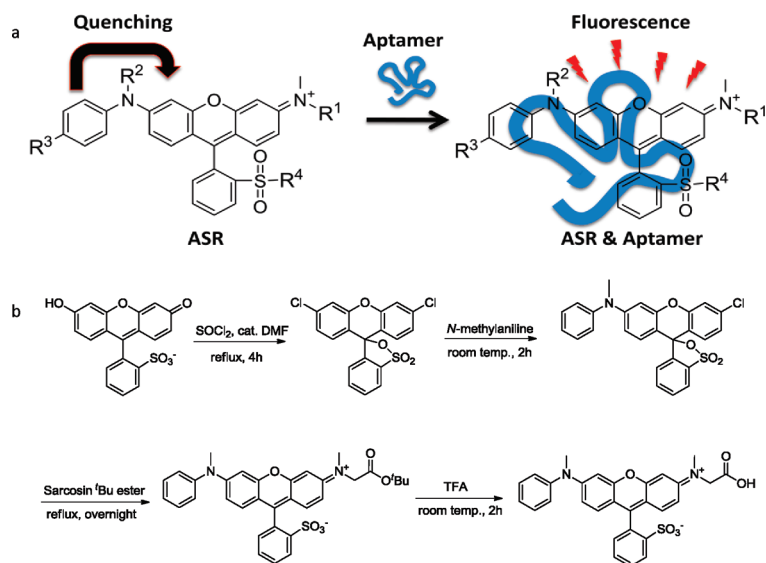


Figure 1. Design and synthesis of ASR fluorogenic probes for RNA tagging. **a** The general structure of ASR and the scheme for the fluorescence enhancement of ASR by RNA aptamer binding ($R_1 = \text{CH}_2\text{CO}_2^-$, $R_2 = \text{Me}$, $R_3 = \text{H}$, $R_4 = \text{O}^-$ for ASR 1 as the SELEX target). **b** Synthetic scheme of the ASR 1 preparation.

live-cell imaging. To address these challenges, we have developed a trans-splicing ribozyme based approach that offers high sensitivity for imaging target RNA molecules through signal amplification (20). Guided by the complementary oligonucleotides, the RNA reporter will generate an mRNA of a reporter enzyme (e.g., β -lactamase or firefly luciferase) *via* trans-splicing, which will be translated into reporter enzymes for imaging with their substrates. This approach has been successfully demonstrated with imaging of target RNA in live cells and live animals, but the enzyme-based amplification compromises the ability to reveal the spatial information of target RNA in subcellular locations.

GFPs have also been used for RNA tagging in a genetic fusion with RNA binding proteins (RBPs). The binding of RBPs to the RBP-specific aptamer genetically attached to the target RNA leads to the formation a protein–RNA complex containing GFP as the fluorescent tag. Several pairs of RBPs and RNA aptamers have been reported with GFP or split GFP (21, 22) as the fluorescent reporter to study RNA localization (23–26), RNA dynamics (27–29), and transcriptional profiling (28, 30). The size of this genetically encoded tag is generally large, sometimes larger than the RNA itself, which may

result in unnatural restriction of the movement and function of the target RNA.

A small-molecule-based RNA tagging approach has been of enormous interest because of its low molecular weight and the ability to tune its cell permeability and fluorescent property *via* chemical modifications. These small-molecule probes can be designed such that the fluorescence is initially quenched but is activated after binding to a specific RNA aptamer, thus promising high sensitivity (6). A number of small-molecule fluorogenic probe and RNA aptamer binding pairs have been reported in the literature (31–36), but these probes have not been successfully demonstrated for live-cell imaging. There is still a strong need for developing new small-molecule probes and discovering RNA aptamers for RNA labeling.

In this paper, we describe our effort toward developing a new set of small-molecule fluorogenic probe and RNA aptamer pairs for RNA labeling. We designed a quenched sulforhodamine analogue (ASR) and performed an *in vitro* SELEX (Systematic Evolution of Ligands by EXponential enrichment) followed by fluorescence screening in *E. coli* to discover an RNA aptamer that can bind the probe ASR and activate its fluorescence with a maximal increase of more than 135-fold in the quantum yield. To elucidate the interaction between the ASR probe and the RNA aptamer, we systematically modified both the ASR structure and the aptamer sequence and identified the structural elements important for binding affinity and fluorescence activation. A rationally designed ASR analogue displayed a 33-fold improvement in the binding affinity compared to the original ASR probe.

RESULTS AND DISCUSSION

Design and Synthesis of the ASR Probe. We derivatized one of the sulforhodamine amino groups with an aromatic moiety aniline, resulting in a quenched, nonfluorescent analogue, aniline-substituted sulforhodamine (ASR). We hypothesized that the binding of an RNA aptamer would activate the fluorescence emission of ASR (Figure 1, panel a). The second amino group of sulforhodamine was alkylated to introduce a carboxylate group for enabling further biotinylation for immobilization on the beads for *in vitro* SELEX selection.

The synthesis of ASR 1 is straightforward as outlined in the Figure 1, panel b (37, 38). The first step involves the conversion of sulfofluorescein to dichlorosulfofluors-

cein. Subsequently, one chloro substituent was displaced by aniline, followed by a second substitution by sarcosine to yield the disubstituted sulforhodamine. ASR **1** shows an absorbance maximum at 555 nm and a very low quantum yield in an aqueous buffer ($\Phi_{\text{Water}} = 0.0017$). The mechanism for quenching the sulforhodamine fluorescence emission is believed to operate through photoinduced electron transfer (PET) (39–42). The electron in the highest occupied molecular orbital (HOMO) of the aniline group in ASR **1** can transfer to the sulforhodamine HOMO and prevent the electron at the excited state of sulforhodamine from returning to its ground state *via* the fluorescence mechanism, resulting in the decrease in the quantum yield of the fluorophore. The PET quenching would become inefficient if the relative geometries of the HOMOs of the fluorophore and aniline are not optimum because of steric restrictions such as the aptamer binding (41). Consistency with this mechanism, the quantum yield of ASR **1** increases by more than 400-fold to 0.71 in 90% glycerol solution (Supplementary Figure 1).

In Vitro SELEX and Fluorescence Screening in *E. coli*.

The selection strategy combines an *in vitro* SELEX affinity screening (Figure 2, panel a) and *E. coli* fluorescence imaging (Figure 2, panel b) to discover aptamers with high binding affinity for ASR **1** and large fluorescence activation.

A library of 100mer RNA aptamers (estimated to be 10^{13}) containing 20 constant nucleotides at each end and 60 randomized nucleotide sequences in the middle was transcribed and mixed with the biotinylated analogue of ASR **1** (Supporting Information) immobilized on the avidin-agarose beads. It was then washed three times with PBS buffer to remove non-bound RNA aptamers and eluted by excess free ASR **1**, followed by reverse transcription and amplification by PCR. The PCR product was then transcribed for the second round of SELEX. These steps were repeated three times to enrich the RNA sequence with high affinity to ASR **1** (43–48).

Next, the selected pool of RNA aptamers was then screened for their light-up property in *E. coli* by fluorescence imaging. Out of approximately 200 bacterial plates that were screened, 35 colonies that displayed strong fluorescence signal (Figure 2, panel b) were sequenced and contained the following nucleotides at the randomized region: GCAGGACCCT CACCTCGGTG ATGATGGAGG GCGCAAGGT TAACCGCCTC AGGTCCTCG

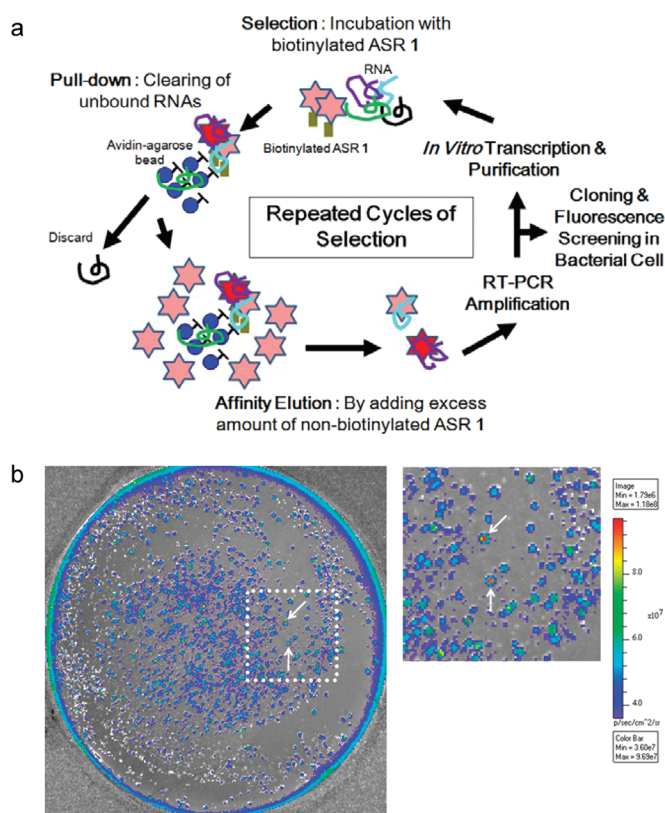


Figure 2. Discovery of ASR binding aptamers *via in vitro* SELEX and *E. coli* fluorescence screening. a) Schematic of the selection strategy. b) Representative fluorescence image of a bacterial plate with 1 μM ASR **1** in the LB Agar gel. Clones containing aptamers that enhance fluorescence of ASR **1** show increased fluorescence signal in the light-tight chamber of an IVIS 200 fluorescence imager; the image at right is an expansion of the selected area containing colonies with the highest fluorescence signal as indicated by white arrows.

The aptamer containing both this randomized sequence and 20mer primer sequences at each end plus additional flanking sequences for cloning into pBK-CMV-eGFP plasmid vector (*Hind*III site *et al.*, see Supplementary Tables 1 and 2 for the definition and primers) is denoted as Apt10L. The M-fold program predicts 4 secondary structures (Figure 3), and the 60 nucleotides randomized sequence in Apt10L is predicted to have two possible secondary structures (Supplementary Figure 2a).

The K_d value and the fluorescence enhancement activity of Apt10L for ASR **1** were determined with fluorescence titration (Figure 4). Fluorescence intensity of ASR **1** at 610 nm increased upon the RNA aptamer binding.

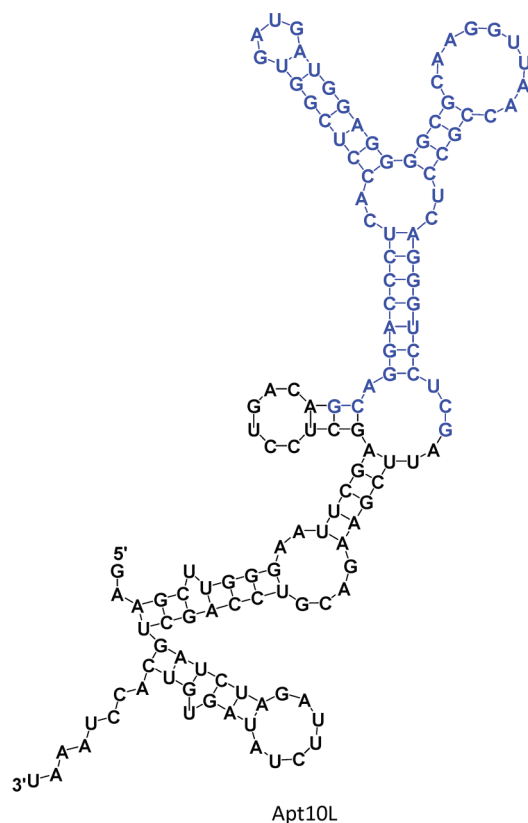


Figure 3. Sequence and representative secondary structure of selected aptamer Apt10L as predicted by the M-fold program; a total of 4 structures are predicted for Apt10L. Sequences in blue represent the region of randomized 60 nucleotides. Apt10L contains long flanking sequences (*HindIII* site *et al.*) on the 5'- and 3'-region for cloning into pBK-CMV-eGFP plasmid vector for fluorescence screening in *E. coli*.

The kinetics of binding between the Apt10L and ASR 1 was rather fast: the fluorescence intensities increased instantaneously to the stable values after mixing during the titration. We found that the method used for preparing Apt10L significantly affected the value of K_d . The K_d value of Apt10L for ASR 1 was $39.1 \pm 7.6 \mu\text{M}$ and F_{max} (expected fluorescence fold enhancement at saturation) was 135 ± 15 (Figure 4, panel a) if Apt10L was purified with a G-25 column without denaturing and renaturing subsequent to *in vitro* transcription. On the other hand, if Apt10L was purified using 6% polyacrylamide-7 M urea gel, which is a common method for RNA purification, the value of K_d was 10-fold lower but the value of F_{max} was much reduced ($K_d = 3.5 \pm 1.5 \mu\text{M}$, $F_{\text{max}} = 29.0$

± 5.1 ; Figure 4, panels c and d). This result may be explained by the fact that after the PAGE purification Apt10L may not refold into the same conformation formed during *in vitro* transcription. Considering that the conformation of *in vitro* transcribed RNA may be closer to its likely structure *in vivo*, we used G-25-purified RNA aptamers for the binding affinity determination in our study.

Mutation and Truncation Analysis To Probe the Interaction between ASR and Apt10L. To understand the interaction between ASR 1 and Apt10L for further optimization of the binding, a systematic truncation and mutation study was performed. We first designed Apt10 M (60mer) with all the flanking sequences but the 60 random sequences removed. In addition, two mutations were introduced at the bottom of its stem region to form two GC base pairs for *in vitro* transcription and for enhanced stabilization of the stem (Figure 5). The K_d value of Apt10 M for ASR 1 was $75.8 \pm 14.3 \mu\text{M}$, and the estimated F_{max} was 125 ± 12.4 (Figure 5). Compared to Apt10L, a mere 2-fold decrease in the binding affinity of Apt10 M indicates that the structure of the randomized sequence area is primarily responsible for the binding to ASR 1.

To examine whether the aptamer binding sequence can be further shortened, Apt10M-54 (54mer) and Apt10M-50 (50mer) variants with three and five less base pairs on the stem regions, respectively, were designed (Figure 5). The binding affinity of these variants for ASR 1 appears to be dependent on the length of the stem: with a shorter stem, the affinity of Apt10M-50 for ASR 1 decreased by 2-fold in comparison to Apt10M, but the affinity of Apt10M-54 for ASR 1 only slightly reduced and the maximal fluorescence enhancement slightly increased ($K_d = 81.2 \pm 11.2 \mu\text{M}$, $F_{\text{max}} = 136 \pm 15.2$). On the other hand, further increase in the length of the stem did not necessarily increase the binding affinity and fluorescence enhancement. For example, variants Apt10M-66, -70, -76, -80 (Supplementary Figure 2b) all showed a lower affinity for ASR 1 than for Apt10 M except Apt10M-80 that displayed a slightly improved binding affinity but a reduced F_{max} value (Supplementary Figure 3a).

Both of the two stem-loop structures in Apt10 M are required for ASR binding and fluorescence activation. Deleting either stem-loop abolished the binding activity of the mutants (Apt10M-S1 and Apt10M-S2) (Figure 6). Mutants Apt10M-Lm2 (the size of the right loop was de-

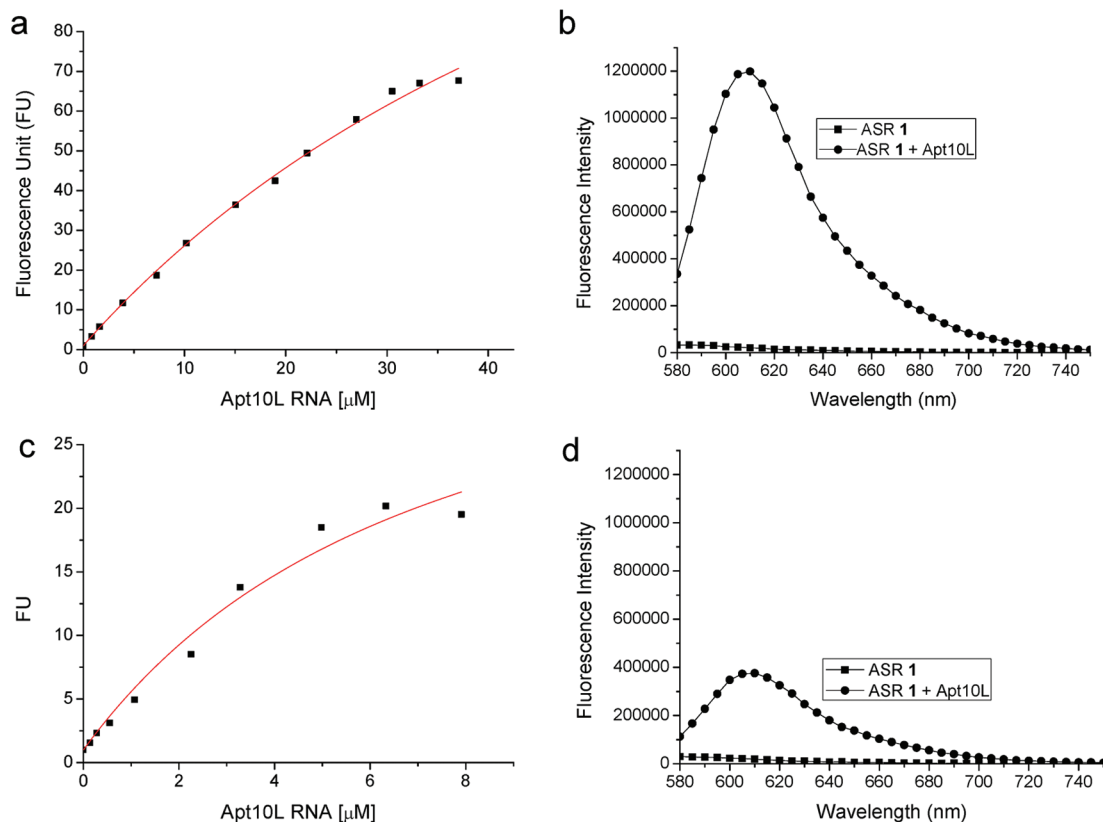


Figure 4. Fluorescence titration of Apt10L RNA aptamer against ASR 1 (1 μM) in PBS buffer (pH 7.4) containing 1 mM MgCl_2 . Excitation and emission wavelength were 555 and 610 nm, respectively. **a)** The K_d value of Apt10L against ASR 1 is $39.1 \pm 7.6 \mu\text{M}$ and F_{max} (expected fluorescence enhancement at saturation) is 135 ± 15 . Fluorescence intensity was normalized as fluorescence unit (FU) against the fluorescence intensity of ASR 1 in the absence of RNA. **b)** Fluorescence spectrum of ASR 1 in the absence or presence of several tens of μM Apt10L RNA. 610 nm is the maximum peak after RNA binding. **c** and **d)** Fluorescence titrations were carried out using PAGE (6% polyarylamide-7 M urea gel) purified Apt10L RNA at the same experimental conditions as in panels **a** and **b**. The K_d value of Apt10L against ASR 1 is $3.5 \pm 1.5 \mu\text{M}$, and F_{max} is 29.0 ± 5.1 .

created by deleting 5 nucleotides in the middle) and Apt10M-Lm3 (the left loop was replaced by the right loop) displayed undetectable fluorescence enhancement upon the addition of ASR 1, further suggesting the cooperative interaction between the two stem-loop structures (Figure 6).

The binding of Apt10 M to ASR 1 is highly sensitive to mutations in the stem-loop region. Single or double mutations were introduced to stabilize the representative secondary structures as predicted by the M-fold program, for example, Apt10M1 (containing mutations G27C and A51C), Apt10M2 (containing a mutation C50A), and Apt10M-Lm1 (containing a U39A mutation on the loop region) (Figure 6). All of these mutants either

do not bind to ASR 1 or have a largely reduced affinity, suggesting the specific interaction with ASR 1 through the loop.

Influence of Flanking Sequence on the Binding. The M-fold program predicts several secondary structures for Apt10L (Supplementary Figure 2a), suggesting that the Apt10L structure is unstable and flexible and that this structural instability could affect its binding affinity to ASR. We examined the role of the flanking sequence on the binding affinity by designing truncated Apt10L variants (T variants). The deletion of some of the flanking sequences decreases the possibility of forming multiple secondary structures. Each of the three Apt10T variants (with the total length of 108, 107, and 88

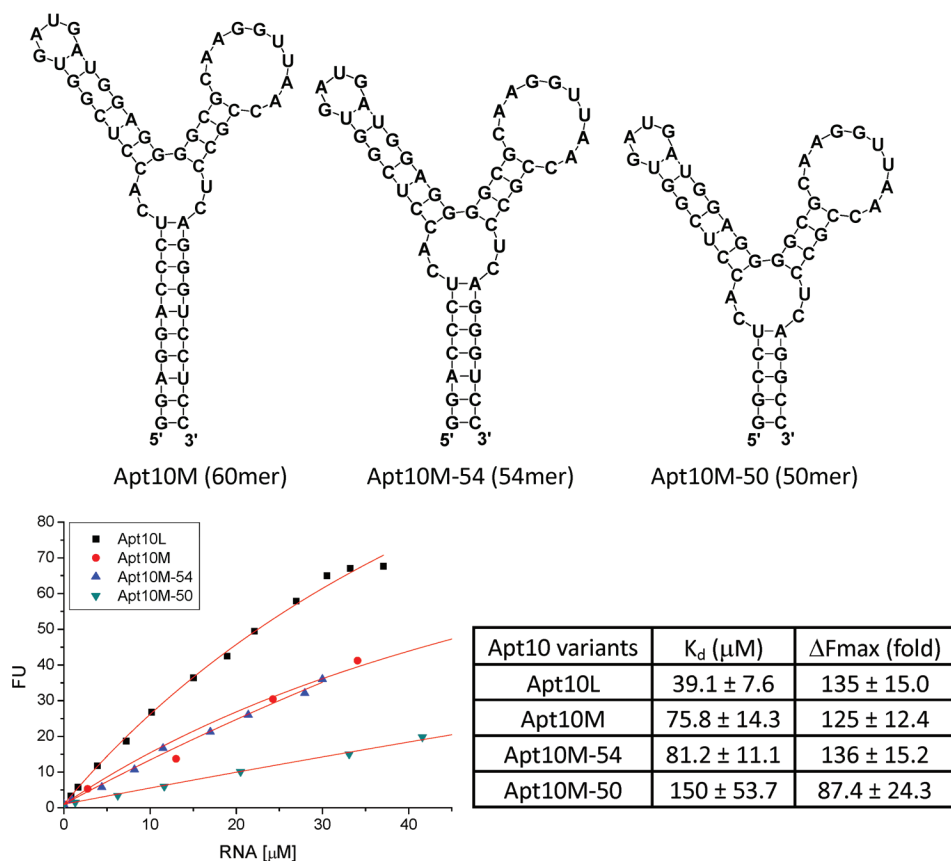


Figure 5. Fluorescence titration of Apt10 M variants against ASR 1 ($1 \mu\text{M}$) in PBS buffer (pH 7.4) containing 1 mM MgCl_2 . Excitation and emission wavelengths were 555 and 610 nm, respectively.

nucleotides) has similar binding affinity to ASR 1 compared to Apt10L (Supplementary Figures 2c and 3b), suggesting that the flanking sequences have only an insignificant effect on the binding affinity.

Mutations were also made in the flanking sequence to strengthen the base-pairing on the stems of each conformation of Apt10L predicted by the M-fold program to stabilize these secondary structures. Both Apt10L1 and Apt10L2 (each with 2 or 3 mutations in the flanking sequences, respectively; Supplementary Figure 2a) showed an identical affinity compared to the Apt10L whereas the Apt10L3 with four mutations showed a 2-fold decrease in the binding affinity (Supplementary Figure 3c). These results further suggest that the interaction of the flanking sequence to the ASR 1 is not as specific as that in the randomized region, although overall these flanking sequences contribute to a 2-fold increase in the binding affinity.

Improvement of K_d and Light-Up Activity by ASR Analogues. To identify the functional groups on ASR 1 that interact with the aptamer, we systematically varied the substitutions on the two amino groups and sulfonate group on ASR 1 to generate a series of analogues. A similar fluorescence titration assay was carried out in the presence of each ASR analogue at $1 \mu\text{M}$ to estimate its binding affinity with Apt10L (Figure 7).

The elimination of the carboxylate group on ASR 1 and the replacement of the methyl group with a diethyl substitution on the amine led to a 3-fold increase in the binding affinity ($K_d = 13.0 \pm 1.1 \mu\text{M}$, $F_{\text{max}} = 80.6 \pm 3.3$ for ASR 2). A substitution of the methyl group on the other amine with an ethyl group produces another 2-fold increase in the binding affinity but a largely reduced F_{max} ($K_d = 6.3 \pm 0.5 \mu\text{M}$, $F_{\text{max}} = 46.7 \pm 1.4$ for ASR 3). Interestingly, the introduction of a methoxy group to the quencher moiety, aniline, of ASR 4 abolished the light-up activity, although the

quenching effect still remains; it confirms that the quencher moiety provides one of the interaction sites for the Apt10L binding and fluorescence activation.

A long tetra(ethylene glycol) group introduced on ASR 5 showed minimal effects on the K_d , which is consistent with the SELEX experiment design that used an ASR analogue biotinylated at the same position as ASR 5. ASR 3 and 6 share similar structures except that the sulfonate group is converted to sulfonamide in ASR 6. This conversion results in a 6-fold decrease in the binding affinity, suggesting that the sulfonate group is also in some contact with Apt10L.

These results suggest that, consistent with our design, both methyl aniline group and the sulfonate-substituted benzene make important contacts with Apt10L, resulting in the fluorescence activation after binding. On the basis of these observations, we designed ASR 7 as an improved analogue (Figure 8), which

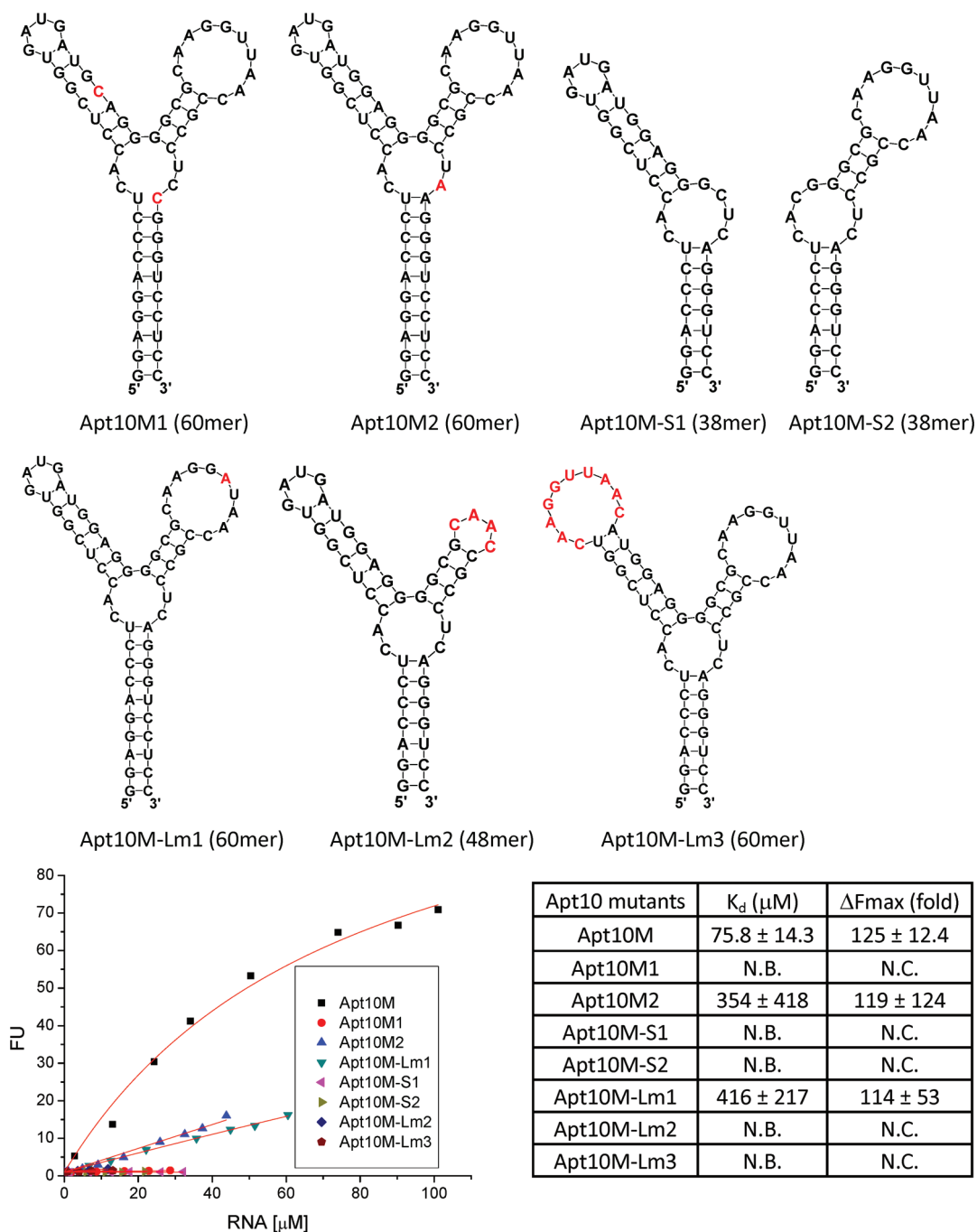


Figure 6. Fluorescence titration of Apt10 M mutants against ASR 1 ($1 \mu\text{M}$) in PBS buffer (pH 7.4) containing 1 mM MgCl_2 . Excitation and emission wavelength were 555 and 610 nm, respectively. N.C.: not calculable. N.B.: no binding. Nucleotides in red stand for mutations.

has a substitution on the amine moiety in the same manner as ASR 2 and a biaryl quencher to increase the

contact interface with the aptamer. Indeed, ASR 7 showed a 33-fold increase in the binding affinity for

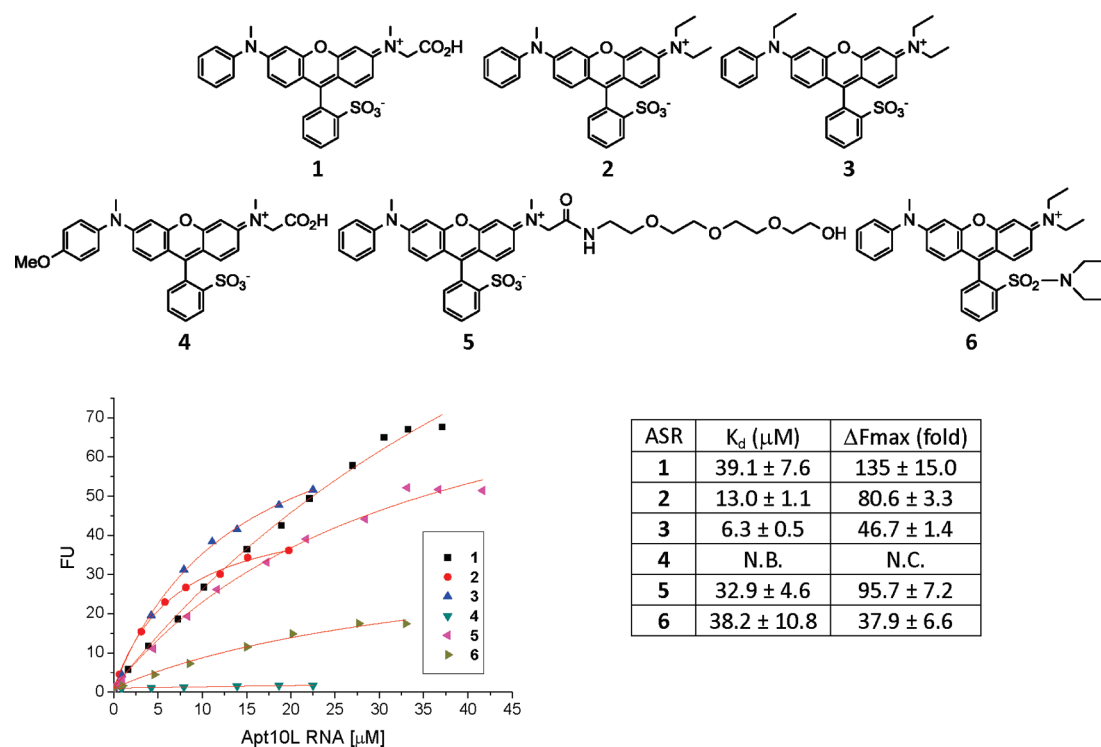


Figure 7. Fluorescence titration of Apt10L against ASR analogues ($1 \mu\text{M}$) in PBS buffer (pH 7.4) containing 1 mM MgCl_2 . Excitation and emission wavelength were 555 and 610 nm, respectively. N.C.: not calculable. N.B.: no binding.

Apt 10 L compared to that of ASR 1 ($K_d = 1.2 \pm 0.1 \mu\text{M}$, $F_{\text{max}} = 88.6 \pm 1.7$ for ASR 7). In addition, ASR 7 binds tightly to Apt10 M with an affinity 2-fold lower than that

of Apt10L ($K_d = 2.6 \pm 0.2 \mu\text{M}$, $F_{\text{max}} = 95.1 \pm 1.5$), as is the case with ASR 1. Despite the highly improved binding affinity by the introduction of a biaryl quencher,

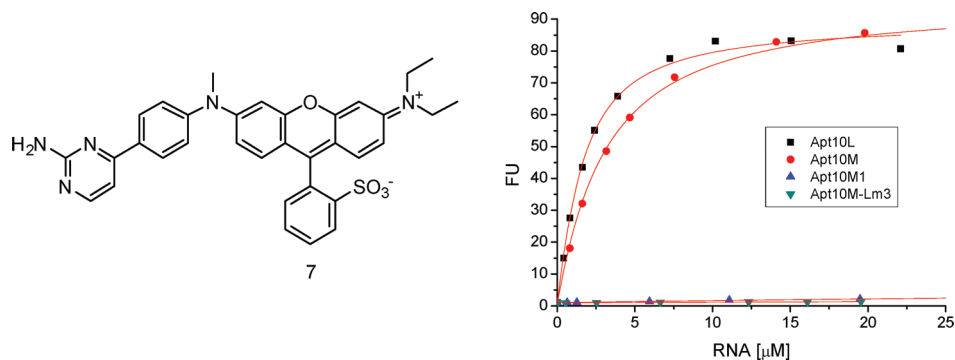


Figure 8. ASR 7 containing a biaryl quencher has a highly improved binding affinity for Apt10L. Fluorescence titration was carried out in PBS buffer (pH 7.4) containing 1 mM MgCl_2 . Increasing concentrations of Apt10L RNA or selected Apt10 M variants (Apt10M, Apt10M1, or Apt10M-Lm3) were added in the presence of $1 \mu\text{M}$ ASR 7. Excitation and emission wavelength were 555 and 610 nm, respectively. K_d of ASR 7 for Apt10L RNA is $1.2 \pm 0.1 \mu\text{M}$, and the F_{max} value is 88.6 ± 1.7 . K_d of ASR 7 for Apt10 M RNA is $2.6 \pm 0.2 \mu\text{M}$, and the F_{max} value is 95.1 ± 1.5 . Like ASR 1, ASR 7 does not bind Apt10M1 and Apt10M-Lm3 mutants, suggesting that the binding specificity is not affected by the introduction of a biaryl quencher.

ASR 7 does not bind to mutants like Apt10M1 and Apt10M-Lm3, suggesting that the binding specificity was not affected by a biaryl quencher. This result indicates that rational modifications of these functional groups on ASR effectively improve the binding affinity to aptamer and fluorogenic properties.

Both the binding affinity and fluorescence activation with ASR 7 and Apt10L compare well to previously reported fluorogen-RNA aptamer pairs (31–36) whose binding constants range from tens of μM to sub- μM , and whose fluorescence increase is generally less than 100-fold with the exception that malachite green displays 2360-fold. Through mutation and truncation analysis and chemical modifications, we have gained a better understanding of the structural interactions between the ASR fluorogen and the aptamer, which can guide us in continuous optimization to further improve both the binding affinity and the fluorescence activation in this new RNA labeling pair.

In summary, we report here a new small-molecule fluorogen and RNA aptamer pair for RNA labeling. The SELEX procedure and fluorescence screening in *E. coli* have been applied to discover the aptamer that can specifically activate the fluorogen. The systematic mutation and truncation study on the aptamer structure determined the minimum binding domain of aptamer specificity to the fluorogen. A series of rationally modified fluorogen analogues have been made to probe the interacting groups of the fluorogen with the aptamer. These results allow us to design ASR 7, which displayed a 33-fold increase in the binding affinity for the selected aptamer compared to original ASR 1 and an 88-fold increase in the fluorescence emission after the aptamer binding. The further refining of the probe structure and aptamer selection could eventually lead to an ideal labeling pair that can be used for *in vivo* RNA live-cell imaging.

METHODS

Synthesis. Detailed synthetic procedures and characterizations of all fluorophores ASR 1–7 are described in Supporting Information.

Quantum Yield Determination. The quantum yield of the ASR (Φ_x) dye was determined relative to the known standard dye rhodamine B ($\Phi_{st} = 0.31$) (37). The integrated fluorescence emission of the ASR dye in 90% glycerol (w/v) with refractive index $n_x = 1.45839$ (49) and rhodamine B in water with refractive index $n_{st} = 1.00$ was plotted against the absorbance to measure slope of the plot for rhodamine B (m_{st}) and ASR (m_x). The quantum yield of the ASR was obtained by using the slopes of the plot in the following formula: $\Phi_x = \Phi_{st}(m_x/m_{st})(n_x/n_{st})^2$.

RNA Preparation. DNA templates for the random N60 library with 20 flanking primer sequences were ordered from Integrated DNA Technologies (see Supplementary Figure 2 for the list of primers). The template was amplified by standard PCR using forward primer containing T7 RNA polymerase promoter and reverse primer in standard GoTaq green solution by promega. The PCR product was purified by QIAprep Spin Miniprep Kit from QIAGEN. The PCR product was transcribed into RNA using *in vitro* RNA transcription kit (T7 Ribo Max; Promega). The transcribed RNA was purified by G-25 spin column (GE healthcare). The purified RNA was quantified by measuring its UV absorption (expected $\epsilon_{260} = 972,100 \text{ L M}^{-1} \text{ cm}^{-1}$).

RNA Selection (SELEX). A biotin-conjugated analogue of ASR 1 was synthesized as described in Supporting Information. It was then immobilized on avidin-agarose beads and incubated with *in vitro* transcribed library (random 60mer), washed three times with PBS, and subsequently reverse transcribed by PCR. The PCR product was transcribed into RNA that was used in the second round of SELEX. After four rounds of enrichment, an aptamer library with high affinity to ASR 1 was generated from the original RNA pool containing about 10^{13} random sequences. The RT-PCR products from this secondary aptamer library were then cloned into pBK-CMV-eGFP vector using restriction enzyme *HindIII* and *XbaI* and transformed into competent *E. coli* cells. Under the lac promoter on the vector, the RNA aptamers will be transcribed in the *E. coli* and will subsequently bind to the cell membrane permeable probe. If the aptamers can functionally

enhance fluorescence intensity of the probe, the clones containing these aptamers will be captured in the light-tight chamber of an IVIS 200 fluorescence imager. After validation of the affinity and light-up activity of the aptamers isolated from the positive colonies by *in vitro* titration, the plasmids containing these aptamers were sequenced.

In Vitro RNA Fluorescence Measurement. Fluorescence titration was carried out in PBS buffer (pH 7.4) containing 1 mM MgCl_2 using Horiba FluoroMax-3 fluorometer. Increasing concentrations of Apt10L variants were added in the presence of each ASR analogue at 1 μM . The concentration of ASR was calculated by measuring absorption at 555 nm (for example, extinction coefficient of ASR 1 was determined to be $75,000 \text{ M}^{-1} \text{ cm}^{-1}$). Maximal excitation and emission wavelength were 555 and 610 nm, respectively.

Determination of Dissociation Constants and F_{max} . Dissociation constant K_d (in μM) was determined by measuring fluorescence intensity (F) versus concentration of the aptamer ($[\text{RNA}]$ in μM) at 1 μM dye concentration. The result was analyzed by the nonlinear fit function of OriginPro 8 using the formula

$$F = \frac{F_{\text{max}}((1 + [\text{RNA}] + K_d) - \sqrt{(1 + [\text{RNA}] + K_d)^2 - 4[\text{RNA}]})}{2} + F_0 \quad (1)$$

where F_{max} = fluorescence intensity at infinite RNA concentration in μM , and F_0 = fluorescence intensity at 0 μM RNA.

Acknowledgment: This work has been supported by a Young Investigator Award from Human Science Frontier Program and a research grant from NIGMS (1R01GM086196-01).

Supporting Information Available: This material is available free of charge via the Internet at <http://pubs.acs.org>.

REFERENCES

1. Tsien, R. Y. (1998) The green fluorescent protein, *Annu. Rev. Biochem.* 67, 509–544.
2. Marks, K. M., and Nolan, G. P. (2006) Chemical labeling strategies for cell biology, *Nat. Methods* 3, 591–596.

3. Johnsson, N., and Johnsson, K. (2007) Chemical tools for biomolecular imaging, *ACS Chem. Biol.* **2**, 31–38.
4. Fernandez-Suarez, M., and Ting, A. Y. (2008) Fluorescent probes for super-resolution imaging in living cells, *Nat. Rev. Mol. Cell Biol.* **9**, 929–943.
5. Dragulescu-Andrasi, A., and Rao, J. (2007) Chemical labeling of protein in living cells, *ChemBioChem* **8**, 1099–1101.
6. Tyagi, S. (2009) Imaging intracellular RNA distribution and dynamics in living cells, *Nat. Methods* **6**, 331–338.
7. Holt, C. E., and Bullock, S. L. (2009) Subcellular mRNA localization in animal cells and why it matters, *Science* **326**, 1212–1216.
8. Gang Bao, W. J. R., and Tsourkas, Andrew (2009) Fluorescent probes for live-cell RNA detection, *Annu. Rev. Biomed. Eng.* **11**, 25–47.
9. Paillason, S., vandeCorput, M., Dirks, R. W., Tanke, H. J., RobertNicoud, M., and Ronot, X. (1997) In situ hybridization in living cells: Detection of RNA molecules, *Exp. Cell Res.* **231**, 226–233.
10. Molenaar, C., Marras, S. A., Slats, J. C. M., Truffert, J. C., Lemaitre, M., Raap, A. K., Dirks, R. W., and Tanke, H. J. (2001) Linear 2' O-methyl RNA probes for the visualization of RNA in living cells, *Nucleic Acids Res.* **29**, e89.
11. Molenaar, C., Abdulle, A., Gena, A., Tanke, H. J., and Dirks, R. W. (2004) Poly(A)(+) RNAs roam the cell nucleus and pass through speckle domains in transcriptionally active and inactive cells, *J. Cell Biol.* **165**, 191–202.
12. Dirks, R. W., and Tanke, H. J. (2006) Advances in fluorescent tracking of nucleic acids in living cells, *Biotechniques* **40**, 489–496.
13. Dirks, R. W., Molenaar, C., and Tanke, H. J. (2001) Methods for visualizing RNA processing and transport pathways in living cells, *Histochem. Cell Biol.* **115**, 3–11.
14. Tyagi, S., Marras, S. A. E., and Kramer, F. R. (2000) Wavelength-shifting molecular beacons, *Nat. Biotechnol.* **18**, 1191–1196.
15. Tyagi, S., and Kramer, F. R. (1996) Molecular beacons: Probes that fluoresce upon hybridization, *Nat. Biotechnol.* **14**, 303–308.
16. Tyagi, S., Bratu, D. P., and Kramer, F. R. (1998) Multicolor molecular beacons for allele discrimination, *Nat. Biotechnol.* **16**, 49–53.
17. Tyagi, S., and Alsmadi, O. (2004) Imaging native beta-actin mRNA in motile fibroblasts, *Biophys. J.* **87**, 4153–4162.
18. Franzini, R. M., and Kool, E. T. (2009) Efficient nucleic acid detection by templated reductive quencher release, *J. Am. Chem. Soc.* **131**, 16021–16023.
19. Silverman, A. P., and Kool, E. T. (2006) Detecting RNA and DNA with templated chemical reactions, *Chem. Rev.* **106**, 3775–3789.
20. So, M. K., Gowrishankar, G., Hasegawa, S., Chung, J. K., and Rao, J. (2008) Imaging target mRNA and siRNA-mediated gene silencing in vivo with ribozyme-based reporters, *ChemBioChem* **9**, 2682–2691.
21. Valencia-Burton, M., McCullough, R. M., Cantor, C. R., and Brude, N. E. (2007) RNA visualization in live bacterial cells using fluorescent protein complementation, *Nat. Methods* **4**, 421–427.
22. Ozawa, T., Natori, Y., Sato, M., and Umezawa, Y. (2007) Imaging dynamics of endogenous mitochondrial RNA in single living cells, *Nat. Methods* **4**, 413–419.
23. Beach, D. L., Salmon, E. D., and Bloom, K. (1999) Localization and anchoring of mRNA in budding yeast, *Curr. Biol.* **9**, 569–578.
24. Bertrand, E., Chartrand, P., Schaefer, M., Shenoy, S. M., Singer, R. H., and Long, R. M. (1998) Localization of ASH1 mRNA particles in living yeast, *Mol. Cell* **2**, 437–445.
25. Kloc, M., Zearfoss, N. R., and Etkin, L. D. (2002) Mechanisms of subcellular mRNA localization, *Cell* **108**, 533–544.
26. Singer, R. H. (2003) RNA localization: Visualization in real-time, *Curr. Biol.* **13**, R673–R675.
27. Forrest, K. M., and Gavis, E. R. (2003) Live imaging of endogenous RNA reveals a diffusion and entrapment mechanism for nanos mRNA localization in *Drosophila*, *Curr. Biol.* **13**, 1159–1168.
28. Fusco, D., Accornero, N., Lavoie, B., Shenoy, S. M., Blanchard, J. M., Singer, R. H., and Bertrand, E. (2003) Single mRNA molecules demonstrate probabilistic movement in living mammalian cells, *Curr. Biol.* **13**, 161–167.
29. Shav-Tal, Y., Singer, R. H., and Darzacq, X. (2004) Imaging gene expression in single living cells, *Nat. Rev. Mol. Cell Biol.* **5**, 855–862.
30. Janicki, S. M., Tsukamoto, T., Salghetti, S. E., Tansey, W. P., Sachidanandam, R., Prasanth, K. V., Ried, T., Shav-Tal, Y., Bertrand, E., Singer, R. H., and Spector, D. L. (2004) From silencing to gene expression: Real-time analysis in single cells, *Cell* **116**, 683–698.
31. Babendure, J. R., Adams, S. R., and Tsien, R. Y. (2003) Aptamers switch on fluorescence of triphenylmethane dyes, *J. Am. Chem. Soc.* **125**, 14716–14717.
32. Constantin, T. P., Silva, G. L., Robertson, K. L., Hamilton, T. P., Fague, K., Waggoner, A. S., and Armitage, B. A. (2008) Synthesis of new fluorogenic cyanine dyes and incorporation into RNA fluoromodules, *Org. Lett.* **10**, 1561–1564.
33. Pei, R., Rothman, J., Xie, Y. L., and Stojanovic, M. N. (2009) Light-up properties of complexes between thiazole orange-small molecule conjugates and aptamers, *Nucleic Acids Res.* **37**, e59.
34. Sparano, B. A., and Koide, K. (2005) A strategy for the development of small-molecule-based sensors that strongly fluoresce when bound to a specific RNA, *J. Am. Chem. Soc.* **127**, 14954–14955.
35. Wilson, C., and Szostak, J. W. (1998) Isolation of a fluorophore-specific DNA aptamer with weak redox activity, *Chem. Biol.* **5**, 609–617.
36. Sando, S., Narita, A., Hayami, M., and Aoyama, Y. (2008) Transcription monitoring using fused RNA with a dye-binding light-up aptamer as a tag: A blue fluorescent RNA, *Chem. Commun.* 3858–3860.
37. Magde, D., Rojas, G. E., and Seybold, P. G. (1999) Solvent dependence of the fluorescence lifetimes of xanthene dyes, *Photochem. Photobiol.* **70**, 737–744.
38. Woodroffe, C. C., Lim, M. H., Bu, W. M., and Lippard, S. J. (2005) Synthesis of isomerically pure carboxylate- and sulfonate-substituted xanthene fluorophores, *Tetrahedron* **61**, 3097–3105.
39. Urano, Y., Kamiya, M., Kanda, K., Ueno, T., Hirose, K., and Nagano, T. (2005) Evolution of fluorescein as a platform for finely tunable fluorescence probes, *J. Am. Chem. Soc.* **127**, 4888–4894.
40. Tanaka, K., Miura, T., Umezawa, N., Urano, Y., Kikuchi, K., Higuchi, T., and Nagano, T. (2001) Rational design of fluorescein-based fluorescence probes, mechanism-based design of a maximum fluorescence probe for singlet oxygen, *J. Am. Chem. Soc.* **123**, 2530–2536.
41. Miura, T., Urano, Y., Tanaka, K., Nagano, T., Ohkubo, K., and Fukuzumi, S. (2003) Rational design principle for modulating fluorescence properties of fluorescein-based probes by photoinduced electron transfer, *J. Am. Chem. Soc.* **125**, 8666–8671.
42. deSilva, A. P., Gunaratne, H. Q. N., Gunnlaugsson, T., Huxley, A. J. M., McCoy, C. P., Rademacher, J. T., and Rice, T. E. (1997) Signaling recognition events with fluorescent sensors and switches, *Chem. Rev.* **97**, 1515–1566.
43. Bartel, D. P., and Szostak, J. W. (1993) Isolation of new ribozymes from a large pool of random sequences, *Science* **261**, 1411–1418.
44. Ellington, A. D., and Szostak, J. W. (1990) In vitro selection of RNA molecules that bind specific ligands, *Nature* **346**, 818–822.
45. Robertson, D. L., and Joyce, G. F. (1990) Selection in vitro of an RNA enzyme that specifically cleaves single-stranded-DNA, *Nature* **344**, 467–468.
46. Sassanfar, M., and Szostak, J. W. (1993) An RNA motif that binds ATP, *Nature* **364**, 550–553.
47. Tuerk, C., and Gold, L. (1990) Systematic evolution of ligands by exponential enrichment - RNA ligands to bacteriophage-T4 DNA-polymerase, *Science* **249**, 505–510.
48. Wilson, C., and Szostak, J. W. (1995) In vitro evolution of a self-alkylating ribozyme, *Nature* **374**, 777–782.
49. http://www.dow.com/glycerine/resources/table12_020.htm.